Membrane and Water Treatment, *Vol. 14, No. 1 (2023) 1-10*
https://doi.org/10.12989/mwt.2023.14.1.001

Thermally-activated *Mactra veneriformis* shells for phosphate removal in aqueous solution

Yeon-Jin Lee[1], Jae-In Lee[2], Chang-Gu Lee[3] and Seong-Jik Park*[1,2,4]

[1]*Department of Bioresources and Rural System Engineering, Hankyong National University, Anseong 17579, Republic of Korea*
[2]*Department of Integrated System Engineering, Hankyong National University, Anseong 17579, Republic of Korea*
[3]*Department of Environmental and Safety Engineering, Ajou University, Suwon 16499, Republic of Korea*
[4]*Institute of Agricultural Environmental Sciences, Hankyong National University, Anseong 17579, Republic of Korea*

(Received October 5, 2022, Revised November 13, 2022, Accepted November 22, 2022)

Abstract. This study explored the feasibility of calcium-rich food waste, Mactra veneriformis shells (MVS), as an adsorbent for phosphate removal, and its removal efficiency was enhanced by the thermal activation process. The CaCO3 in MVS was converted to CaO by thermal activation (>800 °C), which is more favorable for adsorbing phosphate. Thermal activation did not noticeably influence the specific surface area of MVS. The MVS thermally activated at 800 °C (MVS-800), showed the highest phosphate adsorption capacity, was used for further adsorption experiments, including kinetics, equilibrium isotherms, and thermodynamic adsorption. The effects of environmental factors, including pH, competing anions, and adsorbent dosage, were also studied. Phosphate adsorption by MVS-800 reached equilibrium within 48h, and the kinetic adsorption data were well explained by the pseudo-first-order model. The Langmuir model was a better fit for phosphate adsorption by MVS-800 than the Freundlich model, and the maximum adsorption capacity of MVS-800 obtained via the Langmuir model was 188.86 mg/g. Phosphate adsorption is an endothermic and involuntary process. As the pH increased, the phosphate adsorption decreased, and a sharp decrease was observed between pH 7 and 9. The presence of anions had a negative impact on phosphate removal, and their impact followed the decreasing order CO_3^{2-} > SO_4^{2}- > NO_3^{-} > Cl^{-}. The increase in adsorbent dosage increased phosphate removal percentage, and 6.67 g/L of MVS-800 dose achieved 99.9% of phosphate removal. It can be concluded that the thermally treated MVS-800 can be used as an effective adsorbent for removing phosphate.
Keywords: adsorption; calcination; phosphorus; seashell; thermal activation

1. Introduction

Phosphorus (P), largely derived from phosphate rock, is essential for crop growth to support the growing world population (Pan *et al*. 2018). However, excessive phosphorus discharge can cause eutrophication. Eutrophication accelerates the proliferation of algae in water, which has negative effects, such as aquatic oxygen depletion and loss of aquatic plants and organisms (Wang *et al*. 2018), which can pose serious health risks to animals and humans (Bhagowati and Ahamad 2019). High concentrations of phosphorus transported by water and domestic and industrial sewers are discharged into surface water bodies, such as lakes and rivers (Wang *et al*. 2018), and approximately 1.3 million tons of phosphorus are released into water systems worldwide each year (Cheng *et al*. 2018). According to the US Environmental Protection Agency (US EPA), phosphate concentrations should not exceed 0.05 mg/L if a stream discharges into a lake or reservoir, 0.025 mg/L in a stream or runoff that does not discharge into a lake or reservoir, and runoff limit concentrations of 0.1 mg/L. In the European Union (EU), the total concentration of the effluent is limited to 1-2 mg/L depending on the sensitivity of the receiving water (Triantafyllidis *et al*. 2010). Therefore, it is necessary to develop highly effective and economical methods to remove P from wastewater prior to discharge (Xiong *et al*. 2017).

Various physicochemical and biological processes have been investigated for phosphate removal from water and wastewater. These processes include adsorption (Gerke *et al*. 1993, Barron *et al*. 1988), ion exchange (Chen *et al*. 2002), chemical precipitation and coagulation (Ye *et al*. 2010), crystallization and membrane filtration (Kim *et al*. 2008), and reverse osmosis (Luo *et al*. 2016). Among these, reverse osmosis has the disadvantage of being ineffective because its removal efficiency is high, but the treatment cost is also high (Yeoman *et al*. 1988, Clark *et al*. 1997). Chemical precipitation produces sludge and is not preferred for phosphate removal because of the large sludge generation and disposal costs (Morse *et al*. 1998). Biological treatments generally have low removal efficiencies and are sensitive to temperature (Sommariva *et al*. 1997). Beyond these phosphorus removal methods, adsorption is the most efficient method because it is simple, economical, and has the advantage that harmful by-products can be removed with little or no emissions (Liu *et al*. 2013). The aluminum (Al), calcium (Ca), and iron (Fe) contents in phosphate adsorption are closely related to phosphate removal efficiency (Wang *et al*. 2018). Among them, natural materials rich in calcium (Ca) have strong

*Corresponding author, Professor,
E-mail: parkseongjik@hknu.ac.kr

ISSN: 2005-8624 (Print), 2092-7037 (Online)

interactions between some Ca compounds and P. Recently, recycling of wastes or by-products as phosphate adsorbents has received a lot of attention; in particular, shells have shown significant advantages such as high $CaCO_3$ content, non-toxicity, and recyclability (Nguyen *et al*. 2020). For this reason, oyster shells (Lee *et al*. 2021), vongole clam shells (Lo Monaco *et al*. 2012), and mussel shells (Lee *et al*. 2022) have been studied as adsorbents for P removal, but no research has been conducted on *Mactra veneriformis* shells.

M. veneriformis is a marine mollusk belonging to the improved *Clamaceae* family and is a shellfish with a shell length of 45 mm and a height of approximately 30 mm. It inhabits sandy mud or muddy bottoms at a depth of approximately 20 m, is preferred for food, and is distributed all over Korea along the coasts of Japan and China (Yu *et al*. 2009; Ni *et al*. 2015). Thermal-activated mussel shells reduce aqueous phosphate by approximately 90%, and inactivated mussel shells reduce about 40% (Currie *et al*. 2007). Similar to mussels, as the main component is calcium carbonate, *M. veneriformis* shells (MVS) can be an environmentally friendly adsorbent because waste can be recycled as an adsorbent for the phosphate removal process, and the phosphate adsorption capacity can be further improved through thermal activation.

In this study, thermal activation was applied to enhance the adsorption capacity of MVS for phosphates and to remove microorganisms and odors from MVS. The phosphate removal ability and physical/chemical properties of thermally activated MVS at various temperatures were evaluated in batch experiments. Further batch adsorption experiments were performed using the most efficient MVS under various conditions, including reaction time, equilibrium concentration, reaction temperature, pH, competing anion, and adsorbent injection amount.

2. Materials and methods

2.1 Heat treatment method of adsorbent and analysis of adsorbent

MVS used in experiment was obtained from a local restaurant, cleaned with distilled water, and dried at 150 °C for 24 h. After washing, the dried MVS was crushed and sifted to form a constant particle size of 0.245 mm or less before use. The prepared MVS was thermally activated in a muffle furnace (CRFT 830S, Dongseo Science Co. Ltd. Korea) for 4 h to enhance its adsorption capacity. During thermal activation, N_2 gas flowed into the furnace to create anoxic conditions, and the temperatures used for thermal treatment were 100, 300, 500, 700, 800, and 900 °C. The MVS thermally activated at various temperatures are denoted as MVS-NT (untreated), MVS-100, MVS-300, MVS-500, MVS-700, MVS-800, and MVS-900.

MVS thermally-activated at 0–900 °C has been characterized using various methods. The surface morphology of MVS was observed using a field-emission scanning microscope (FE-SEM; S-4700, Hitachi, Japan). The composition and spatial distribution of the elements on the sample surface were investigated using an energy dispersive X-ray spectrometer (EDS) attached to the FE-SEM. The specific surface area of MVS was calculated using the Brunauer-Emmett-Teller equation from the nitrogen adsorption-desorption isotherm data obtained using a surface area analyzer (Autosorb-iQ, Quantachrome Corporation, USA). The mineralogical structure of the adsorbent was analyzed using X-ray diffraction (XRD) (Smartlab, Rigaku, Japan). X-ray fluorescence spectroscopy (XRF; Primus ZSX 4, Rigaku, Japan) was used to analyze the elemental composition of the MVS annealed at various temperatures. The mass change according to the temperature change of the sample was analyzed using a thermogravimetric analyzer (TGA; Pyris1, Perkin-Elmer, USA).

2.2 Adsorption experiment

The phosphate stock solution used in the experiment was prepared by dissolving potassium monohydrogen phosphate (K_2HPO_4) and potassium dihydrogen phosphate (KH_2PO_4) in deionized water to obtain 1000 mg/L, which was diluted according to the required concentration. To investigate the phosphorus adsorption capacity of MVS according to the thermal activation temperature, 30 mL of 100 mg/L phosphate solution and 0.1 g of untreated MVS (MVS-NT) and thermally activated MVS (MVS-100, MVS-300, MVS-500, MVS-700, MVS-800, and MVS-900) were used to investigate the phosphorus adsorption capacity of MVS according to the thermal activation temperature.

The MVS-800 was subjected to batch testing under various experimental conditions. Unless otherwise specified, all adsorption experiments were performed at a reaction temperature of 25 °C with 3.33 g/L of MVS-800 and a phosphate solution at a concentration of 900 mg/L with stirring at 100 rpm for 48 h. For the kinetic adsorption of MVS-800, a phosphate concentration of 900 mg/L was used. In addition, at a reaction temperature of 25 °C, various reaction times were carried out in the range of 0.25 to 92 h (0.25, 0.5, 1, 2, 3, 6, 12, 24, 48, 72, up and 92 h). Equilibrium adsorption of MVS-800 was performed for 48 h at initial phosphate concentrations of 10, 30, 50, 100, 300, 400, 500, 700, 900, 1000, 1200, and 1300 mg/L. Thermodynamic adsorption was performed by controlling the reaction temperature at 15 °C, 25 °C, and 35 °C. The effect of pH on the phosphorus adsorption capacity of MVS-800 was evaluated at pH values ranging from 3 to 9. Acidic and basic solutions (HCl and NaOH, 0.1 M) were added to adjust the pH of the solution. NaCl, Na_2SO_4, $NaHCO_3$, and $NaNO_3$ at concentrations of 1.0 mM and 10 mM were used to prepare phosphate solutions containing competing anions, and the effect of competing anions on adsorption was evaluated. The effects of the amount of MVS-800 adsorbent on the phosphate adsorption capacity and removal ratio were evaluated by reacting different amounts of adsorbent (1.67, 3.33, 6.67, 13.33, and 16.67 g/L).

All experiments were repeated thrice. After adsorption, the phosphate solution and adsorbent were separated using filter paper. The concentration of phosphate separated from the adsorbent was measured by the ascorbic acid method

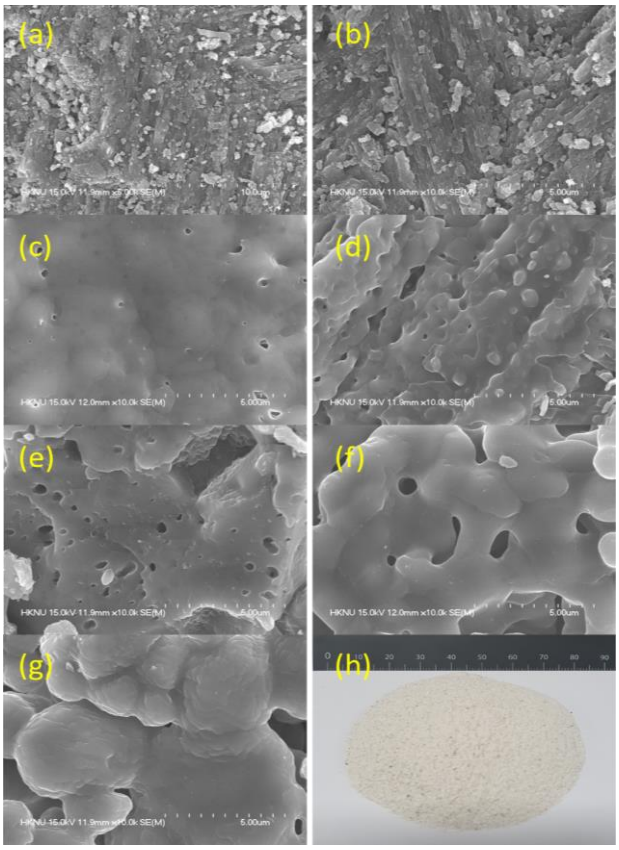

Fig. 1 Surface morphology of the thermal-activated MVS at various temperatures: (a) untreated, (b) 100 °C, (c) 300 °C, (d) 500 °C, (e) 700 °C, (f) 800 °C, (g) 900 °C, and (h) digital image of powdered MVS

(Sağlam *et al*. 2016). The absorbance of the isolated solution was measured at 880 nm using an ultraviolet/ visible spectrophotometer (Optizen POP QX; Mecasys, Korea).

2.3 Data analysis of adsorption kinetic, isotherms, and thermodynamic models

The kinetic model of the pseudo-first-order model (Eq. 1) and pseudo-second-order (Eq. 2) were used to fit the experimental kinetic data.

$$q_t = q_e(1 - \exp(-k_1 t)) \tag{1}$$

$$q_t = \frac{k_2 q_e^2 t}{1 + k_2 q_e t} \tag{2}$$

where q_t is the amount of phosphate adsorbed at time t (mg/g), q_e is the amount of phosphate adsorbed at equilibrium (mg/g), k_1 is the pseudo-first order rate constant (1/h), and k_2 is the pseudo-second order rate constant (g/mg/h).

The equilibrium data were analyzed using the Langmuir (Eq. 3) and Freundlich (Eq. 4) models:

$$q_e = \frac{Q_m K_L C}{1 + K_L C} \tag{3}$$

$$q_e = K_F C_e^{\frac{1}{n}} \tag{4}$$

where C_e is the equilibrium concentration of the phosphate solution (mg/L), Q_m is the maximum adsorption capacity of the adsorbent (mg/g), K_L is the Langmuir constant related to the affinity of the binding energy (L/mg), K_F is the distribution coefficient (L/g), and $1/n$ is the Freundlich constant (-). The values of K_L, Q_m, K_F, and n can be determined by fitting the Langmuir and Freundlich models to the observed data.

Thermodynamic adsorption parameters, such as Gibbs free energy (ΔG^0), enthalpy (ΔH^0), and entropy (ΔS^0), were determined using the following equations:

$$\Delta G^0 = \Delta H^0 - T\Delta S^0 \tag{5}$$

$$\Delta G^0 = -RT \ln K_e \tag{6}$$

$$\ln K_e = \frac{\Delta S^0}{R} - \frac{\Delta H^0}{RT} \tag{7}$$

$$K_e = \frac{\alpha q_e}{C_e} \tag{8}$$

where ΔG^0 is the change in Gibbs free energy, ΔS^0 is the change in entropy, ΔH^0 is the change in enthalpy, T is the absolute temperature (K), R is the universal gas constant (8.314 J/mol · K), K_e is the equilibrium constant, and a is the amount of adsorbent (g/L).

3. Results and discussion

3.1 Adsorption properties and phosphate adsorption capacity of thermally-activated MVS

The physicochemical properties of thermally activated MVS at 0–900 °C were analyzed using various methods. FE-SEM images of thermally activated MVS at various temperatures are shown in Fig. 1. The surface of untreated MVS was observed to have a rough and irregularly layered structure. As the thermal activation temperature increased, the surface of MVS melted, and a smooth surface was observed in MVS-300. Stomata gradually increased from MVS-300 to MVS-700. In MVS-800, the pores became noticeably very large, but the large pores in MVS-900 melted and were destroyed. This shows that the organic matter in MVS is decomposed and released during the thermal activation process, and the surface morphology changes (Lee *et al*. 2022). The specific surface area of MVS did not change with the thermal activation temperature, and the specific surface area of MVS was 3 m^2/g or less. Table 1 shows that the specific surface area of MVS was not dependent on thermal activation. Accordingly, the phosphate adsorption capacity of MVS was not affected by the specific surface area. As shown in Table 1, the elemental composition of MVS changed as the thermal activation temperature of MVS increased. The change in the elemental composition of MVS indicated that the Ca

Table 1 Elemental composition, mineral composition and BET results of thermal-activated MVS at various temperatures

Adsorbent	Mineral composition (%)				Surface area (m^2/g)	Pore volume (cm^3/g)	Pore size (nm)	Elemental Composition (wt%)						
	Calacite $CaCO_3$	Aragonite $CaCO_3$	Graphite-3R	Lime CaO				CaO	C	Na_2O	SiO_2	P_2O_5	Cl	Others
MVS-NT	-	100	-	-	1.24	0.0074	2.39	64.4	29.0	0.96	0.22	0.10	0.05	5.3
MVS-100	-	100	-	-	2.16	0.0091	1.68	67.4	26.0	1.02	0.26	0.08	0.04	5.4
MVS-300	7.04	93.0	-	-	1.70	0.0063	1.50	65.6	28.0	0.99	0.21	0.06	0.04	5.1
MVS-500	98.5	-	1.49	-	0.58	0.0021	1.42	63.4	30.0	1.18	0.27	0.07	0.04	5.0
MVS-700	99.0	-	1.04	-	0.37	0.0018	1.96	63.3	27.0	2.15	0.34	0.07	0.02	7.1
MVS-800	17.97	-	-	82.0	0.45	0.0011	4.78	73.4	20.0	1.32	0.09	0.05	0.03	5.1
MVS-900	5.5	-	-	94.5	0.61	0.0028	1.79	75.3	19.0	0.34	0.11	0.05	0.02	5.2

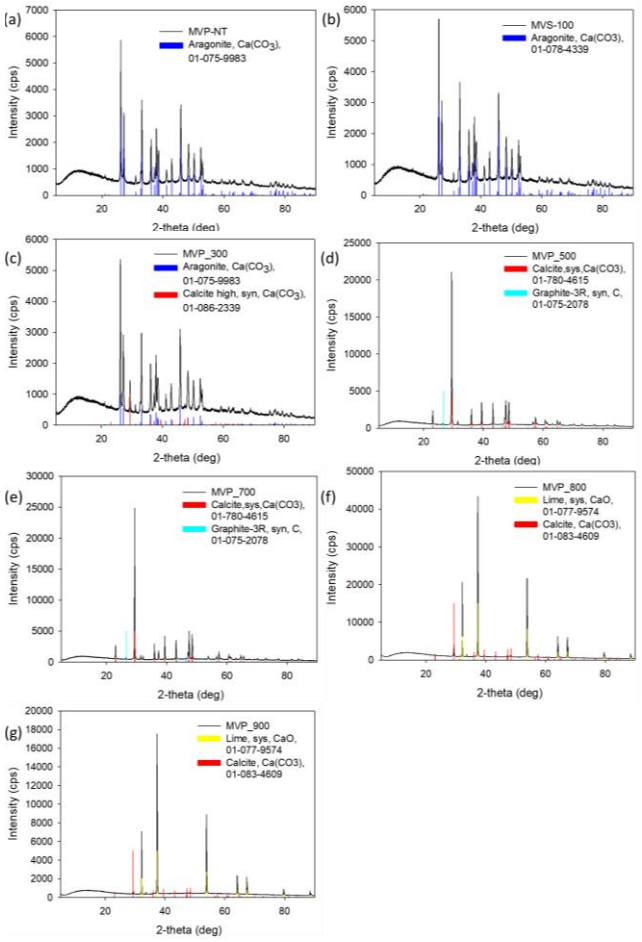

Fig. 2 XRD patterns of the thermal-activated MVS at various temperatures: (a) untreated, (b) 100 °C, (c) 300 °C, (d) 500 °C, (e) 700 °C, (f) 800 °C, and (g) 900 °C

content increased, and the C content decreased as the thermal activation temperature increased. This is because, during the thermal activation process, $CaCO_3$ decomposes into CaO at a high temperature, and CO_2 is released (Choia *et al*. 2021).

The mineral structure of MVS is thermally activated and changes with the temperature. The XRD results are shown in Fig. 2 and Table 1. The peaks of MVS-NT and MVS-100 represent aragonite ($CaCO_3$) and calcite ($CaCO_3$),

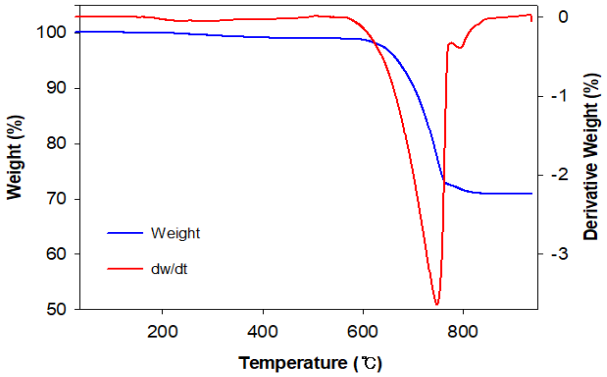

Fig. 3 Weight and derivative weight change of MVS TGA analysis result of increase in MVS with increasing temperature

respectively. MVS-300 had two peaks, aragonite ($CaCO_3$) and calcite ($CaCO_3$), composed of 93.0% and 7.0%, respectively. MVS-500 and MVS-700 had peaks corresponding to calcite ($CaCO_3$) and graphite (Graphite-3R); calcite (98.5% and 99.0%, respectively) is very dominant over graphite (1.5% and 1.0%, respectively). The peaks of aragonite disappeared above 500 °C. The peak of lime (CaO) began to appear in MVS-800, and the calcite ($CaCO_3$) content decreased significantly. As the thermal activation temperature increased to 900 °C, the lime (CaO) content further increased and the calcite ($CaCO_3$) content decreased in MVS-900. This is because, as described above, during the thermal activation process, $CaCO_3$ is decomposed into CaO at a high temperature, and CO_2 is released.

The results of the TGA analysis of mass loss with increasing temperature are shown in Fig. 3. The mass loss with increasing temperature of MVS slowly decreased up to 600 °C with increasing temperature and showed a sharp weight loss between 600 °C and 800 °C. Above 800 °C, there was no change in weight. The weight change between 600 °C and 800 °C decreased from 98.7% to 71.6% because $CaCO_3$ decomposed to CaO and CO_2 between 600 °C and 800 °C (Lee *et al*. 2021). It can be inferred from this result that $CaCO_3$ in MVS starts to decompose at 600 °C and is completely decomposed at 800 °C. These results are consistent with the CaO peak, shown from 800 °C in the

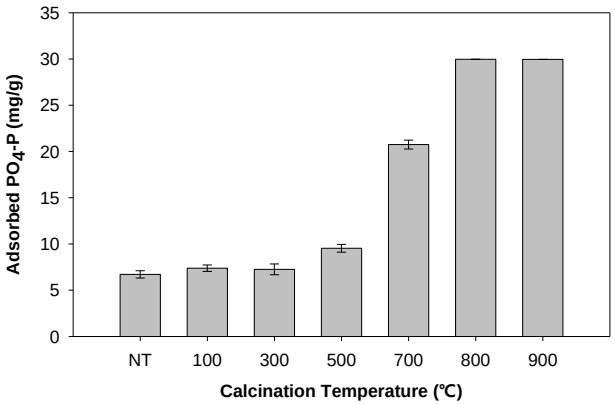

Fig. 4 Phosphorus adsorption capacity of MVS by thermal-activated temperature (initial concentration 100 mg/L)

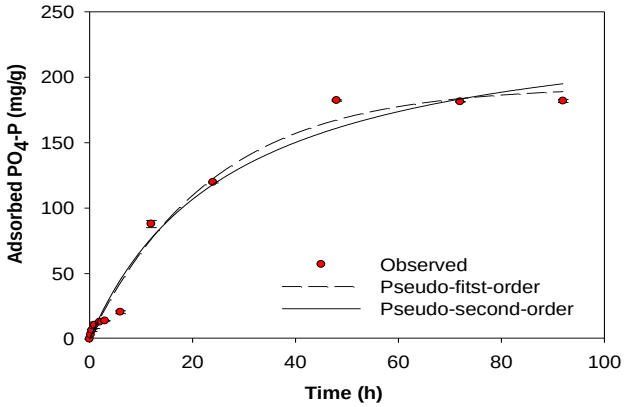

Fig. 5 Phosphate adsorption according to contact time between phosphate solution and MVS-800

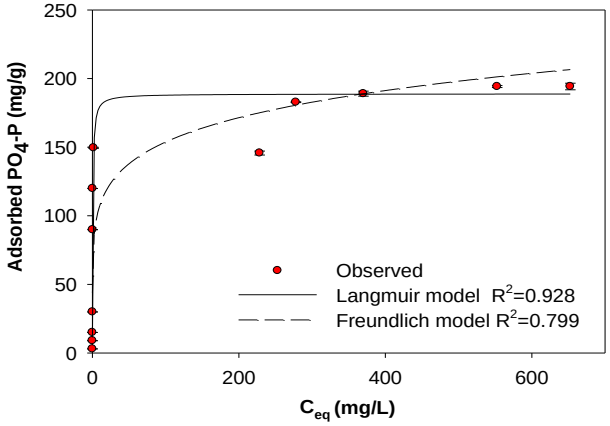

Fig. 6 Equilibrium adsorption to phosphate adsorption of thermally activated MVP at 800 °C

XRD results above, and the elemental composition with decreasing C content and increasing Ca content.

Fig. 4 shows the effect of phosphate adsorption on the MVS according to the activation temperature. The phosphate adsorption capacity was observed from MVS-NT to MVS-500. However, for MVS-700, the adsorption amount increased noticeably from 9.53 mg/g to 20.75 mg/g. Phosphate adsorption showed the greatest adsorption capacity in MVS-800 and MVS-900. Phosphate adsorption by MVS-800 was 29.96 mg/g, and that by MVS-900 was 29.95 mg/g, indicating a slight difference in phosphate adsorption capacity between MVS-800 and MVS-900. The higher phosphate adsorption capacity of MVS-800 and MVS-900 compared to that of MVS-700 can be explained by the CaO that appeared in MVS-800 in the XRD analysis results. CaO is more soluble than $CaCO_3$ (Lee *et al*. 2021) and reacts with H_2O to form $Ca(OH)_2$. $Ca(OH)_2$ reacts with phosphate to form hydroxyphosphate ($Ca_{10}(PO_4)_6(OH)_2$) and calcium phosphate ($Ca_3(PO_4)_2$), which remove phosphate in water via the formation of precipitates. This has been demonstrated for other adsorbents based on $CaCO_3$ (Yin and Kong 2014, Lee *et al*. 2022).

Table 2 Kinetic model parameters obtained from model fitting of experimental data

Model	Parameter		R^2(-)
Pseudo-first-order	q_e (mg/g)	k_1 (1/h)	0.985
	136.06	0.042	
Pseudo-second-order	q_e (mg/g)	k_2 (g/mg/h)	0.977
	253.46	0.0001	

Table 3 Equilibrium model parameters obtained from model fitting of the experimental data

Model	Parameter		R^2(-)
Langmuir	Q_m (mg/g)	K_L (L/mg)	0.93
	188.86	1.91	
Freundlich	K_F (L/g)	1/*n* (-)	0.80
	74.48	0.16	

3.2 Kinetic of phosphate adsorption

Kinetic analyses are essential because they provide insight into the interactions between adsorbents and adsorbates and provide information on the adsorption equilibrium and mechanisms (Dos Reis *et al*. 2020). Therefore, using MVS-800 and 900 mg/L of phosphate solution, kinetic adsorption was investigated for its ability of MVS-800 to adsorb the phosphate solution. The amount of phosphate adsorbed by MVS-800 increased to 119.74 mg/g at 24 h. Thereafter, the adsorption capacity further increased up to 182.20 mg/g at 48 h, in which the adsorption capacity was reached to equilibrium.

To investigate the principle of kinetic adsorption between MVS-800 and phosphate, experimental data were analyzed through pseudo-first-order (PFO) and pseudo-second-order (PSO) models. The kinetic phosphate adsorption data and model-fitted line are shown in Fig. 5, and the parameters of the kinetic models PFO and PSO are listed in Table 2. When the parameters of the two kinetic models are compared, it can be seen that the R^2 value (0.985) of the PFO model is higher than the R^2 value (0.977) of the PSO model. In addition, the adsorption amount of phosphate obtained through the experiment (182.20 mg/g) was closer to that obtained using the PFO

Table 4 Maximum adsorption amount of phosphate adsorbent reported in other literature

Absorbents	Q_m (mg/g)	Particle size	Reference
MVS-800	188.86	≤0.425 mm	This study
BC-LDH composite (B-Mg/Al-LDH-1)	152.1	0.15 mm	(Yang *et al*. 2019)
$NaLa(CO_3)_2$	120.23	13.89 μm	(Hao *et al*. 2019)
Iron-modified biochars derived from waste activated sludg(MB3)	111.00	0.5–1 mm	(Yang *et al*. 2018)
Calcined eggshells	108.20	0.425–0.85 mm	(Lee *et al*. 2022)
Magnetic MLC composites (MLC-21)	77.85	54.21	(Hao *et al*. 2019)
Mg-biochar from ground coffee waste	63.5	3.46 μm	(Shin *et al*. 2020)
Chitosan beads modified with zirconium (ZCB)	61.7	-	(Liu and Zhang 2015)
CSW-T	57.64	-	(Reis *et al*. 2020)
Mesoporous ZrO_2	29.71	-	(Liu *et al*. 2008)
ACF-ZrFe	26.32	-	(Xiong *et al*. 2017)
$ZrO_2@Fe_3O_4$	15.98	-	(Fang *et al*. 2017)
Magnetic Fe-Zr binary oxide	13.65	-	(Long *et al*. 2011)
Hybrid hydrated aluminum oxide zeolite (Z-Al)	7.00	200 μm	(Guaya *et al*. 2015)

model (193.06 mg/g) than that obtained using the PSO model (253.46 mg/g), We found that the PFO model better explains the phosphate adsorption of MVS-800. In addition, the amount of phosphate adsorbed in the actual experiment (182.20 mg/g) was closer to that obtained by analysis with the PFO model (193.06 mg/g) than with that obtained by the PSO model (253.46 mg/g). These results suggest that, among the two kinetic models, the PFO model better explains the phosphate adsorption of MVS-800 than the PSO model. The theoretical interpretation of the pseudo-first-order equations suggests that the overall adsorption process is controlled by the rate of adsorption/desorption in terms of the chemical reaction of the adsorbent surface. (Plazinski *et al*. 2009).

3.3 Adsorption isotherms

Applying the isothermal model to underwater adsorption data helps to investigate the principle mechanism of contaminant adsorption and to design the capacity and conditions for contaminant removal (Dwivedi *et al*. 2015). The Langmuir and Freundlich models were used for experimental isotherm data analysis. The isothermal model was used to analyze the phosphate adsorption capacity of MVS-800 at various concentrations of phosphates (10-1300 mg/L). The parameters of the modeled data are presented in Table 3 and the adsorption data are shown in Fig. 6. The phosphate adsorption capacity of MVS-800 increased with increasing initial phosphate concentration. The R^2 values of the Freundlich is 0.80 and the R^2 of the Langmuir models were 0.93. As a result, the Langmuir R^2 value is higher than the Freundlich R^2 value, indicating that the Langmuir model is a better fit for the phosphate adsorption of MVS-800. The Langmuir model assumes tomographic sorption, in which all surface regions are similar and independent of the adjacent site occupancy (Christou *et al*. 2019); that is, phosphate adsorption suggests that the entire adsorption site is the same on the surface of MVS-800 and that it is a monolayer adsorption with a similar affinity for phosphate (Jiao *et al*. 2021). The adsorption amount in the actual adsorption experiment was 194.22 mg/L, close to the maximum adsorption amount (188.86 mg/g calculated using the Langmuir model.

Table 4 compares the maximum adsorption capacity of phosphate adsorbents of other literature and the maximum adsorption capacity of MVS-800. It can be seen that MVS-800 has a high adsorption capacity among the adsorbents for phosphate removal reported in other literature.

1/n, a parameter of the Freundlich model, is a heterogeneity factor related to the adsorption strength or surface non-uniformity between the adsorbent and adsorbent (Wang *et al*. 2017). Van Bladel and Moreale defined the Freundlich K and 1/n constants as adsorption capacity and intensity, respectively (Shafqat and Pierzynski 2014). A value of 1/n less than 1 indicates a suitable Langmuir isotherm, whereas a value greater than 1 indicates cooperative adsorption (Tan *et al*. 2008). The 1/n value calculated in this study was 0.16. K_F is 74.48 $(mg/g)\cdot(L/g)^{1/n}$.

3.4 Thermodynamics of adsorption

Phosphate adsorption experiments were performed on MVS-800 at different reaction temperatures of 15 °C, 25 °C, and 35 °C, respectively, and thermodynamic analysis was performed. A plot of $\ln(K_e)$ versus 1/T from the intercept is calculated as the change in entropy (ΔS°), and it is possible to calculate the change in enthalpy (ΔH°) by the slope (Lima *et al*. 2019). Table 5 lists the parameters used in the thermodynamic analysis. ΔH° suggests that the adsorption reaction between the solution and the adsorbent is endothermic or exothermic. Entropy is a criterion for the pattern or disorder in which thermodynamic adsorption systems are rearranged, and ΔS° may reflect specific interactions of the adsorbent-adsorbent and the limited

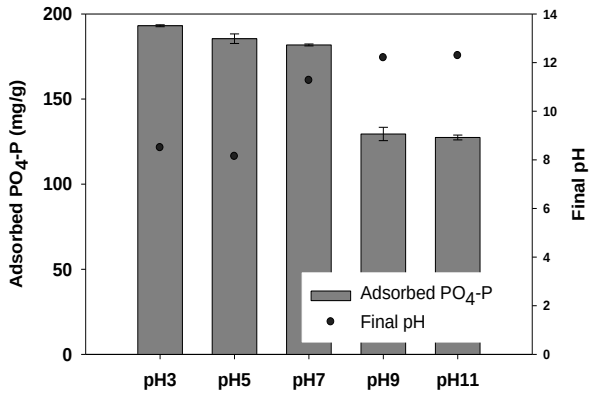

Fig. 7 Effect of phosphate solution pH on Phosphate Adsorption of MVS-800

Table 5 Thermodynamic parameters of adsorption between MVS-800 and phosphate solution

Temperature (°C)	ΔH° (kJ/mol)	ΔS° (J/K mol)	ΔG° (kJ/mol)
15	40.5	112.2	8.22
25			7.10
35			5.98

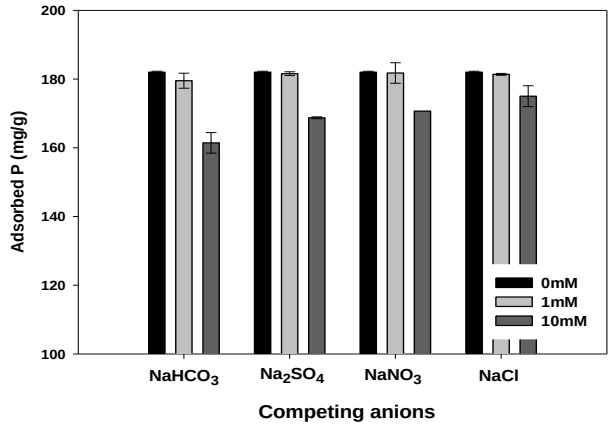

Fig. 8 Effect of coexisting anions on phosphate adsorption of MVS-800

mobility of adsorbed molecules (Du *et al*. 2021). ΔG° spontaneously and can also be used to analyze the type of indicates whether the adsorption process can proceed spontaneously and can also be used to analyze the type of adsorption involved in the reaction (Ren *et al*. 2021). According to the analysis results, it can be seen that the thermodynamic adsorption of phosphate to MVS-800 increases with increasing temperature. Because ΔH° is positive, the adsorption of phosphate in the thermally activated MVS-800 is endothermic. The positive value of ΔS° also shows that the randomness at the interface between solid and solution for phosphate adsorption in the internal structure of MVS-800 increases (Lee *et al*. 2022; Unuabonah *et al*. 2007; Liu *et al*. 2011) ΔG° was 8.22, 7.10 and 5.98 kJ/mol at 15, 25, and 35 °C, respectively, and decreased with increasing temperature. It can be seen that in phosphate adsorption by MVS-800, an involuntary adsorption reaction occurs despite an increase in the reaction temperature for phosphate adsorption.

3.5 Phosphate solution adsorption of MVS-800 according to pH

Changes in pH can affect the adsorption process by dissociating the adsorbate of different species and functional groups present at the active site of the adsorbent (Reis *et al*. 2020). For this reason, it is necessary to understand the effect of pH on the phosphate adsorption process. The adsorption amount of MVS-800 in a phosphate solution of pH 3-11 shows a tendency inversely proportional to the increase in pH. From pH 3 to pH 7, the change was insignificant from 193.08 mg/g to 181.82 mg/g, but the adsorption amount decreased sharply at pH 9 and was maintained at 127.43 mg/g until pH 11. The inorganic forms of P (PO_4-P) in water exist in various anionic forms, such as $H_2PO_4^-$, HPO_4^{2-}, and PO_4^{3-}, depending on environmental pH (Zhang *et al*. 2020). At pH 11, phosphate exists as HPO_4^{2-}, which is thought to be due to the decrease in the phosphate adsorption capacity of MVS-800 owing to electrostatic repulsion with the negatively charged adsorbent surface (Karaca *et al*. 2006). In addition, it was determined that the phosphate adsorption capacity of MVS-800 is lowered due to the competition between OH^- and HPO_4^{2-} in terms of adsorption of MVS-800 because of the presence of a large amount of OH^- due to the high pH. When the pH value is low, the surface of MVS-800 is positively charged, indicating that the adsorption amount is increased. Therefore, the pH condition for the highest adsorption amount of MVS-800 was pH 3, and the pH condition for the lowest adsorption amount was pH 11.

3.6 Effect of competing ions on phosphate adsorption of MVS-800

Surface water and groundwater are frequently polluted with anions, including bicarbonate, sulfate, nitrate, and chloride, commonly supplied by industrial and agricultural operations (Hong *et al*. 2020). Therefore, it is necessary to investigate the effect of anions on phosphate adsorption. The coexisting anions (CO_3^{2-}, SO_4^{2-}, NO_3^-, and Cl^-) in the phosphate solution interfere with phosphate adsorption by MVS-800. As the amount of coexisting anions increased, the amount of phosphate adsorbed by the MVS-800 decreased. In addition, it was found that competing anions had a negative effect on phosphate adsorption in the following order: $CO_3^{2-} > SO_4^{2-} > NO_3^- > Cl^-$. HCO_3^- or SO_4^{2-} combines with Ca^{2+} in MVS-800 to form insoluble or sparingly soluble substances, thereby reducing the number of active sites on the adsorbent surface, which has a significant effect on phosphate removal (Liu *et al*. 2019). Sulfate ions competed with phosphate to occupy the surface of MVS-800, reducing phosphate adsorption. This is because the ionic radius of aqueous sulfate (2.3 Å) is almost the same as that of phosphate (2.38 Å) (Kumar & Viswanathan. 2018). In comparison, NO_3^- and Cl^- had no significant effect on phosphate removal. This is because

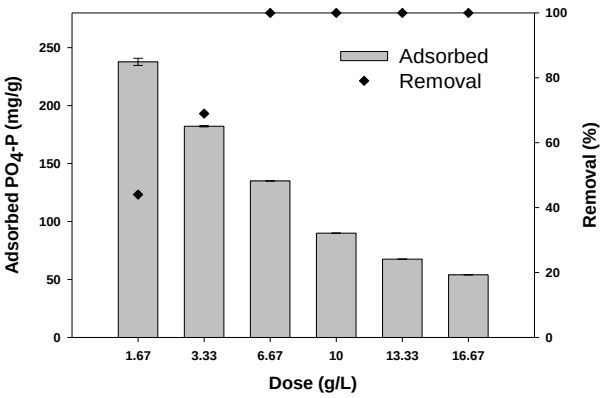

Fig. 9 Effect of MVS-800 dose on phosphate adsorption of MVS-800

phosphate adsorption forms an inner complex and nitrate and chloride adsorption do not compete as they form an outer complex (McBride 1997, Kumar *et al*. 2014).

3.7 Phosphate adsorption according to the dose of MVS-800

The adsorbent dosage is an important parameter that affects the removal efficiency of the adsorbent. The removal efficiency of MVS-800 was proportional to the adsorbent dosage. In addition, the adsorption amount per unit mass decreased as the adsorbent dosage increased in Fig 9. When the adsorbent capacity was increased from 1.67 g/L to 6.67 g/L, the phosphates removal efficiency increased from 44.0% to 99.9%. This is because they provide more adsorption sites at higher adsorption capacities (Nguyen *et al*. 2020). Compared with other phosphate removal references, MVS-800 requires less adsorbent dosage to achieve greater than 90% removal efficiency compared to other adsorbents (Waste brick 20 g/L; (Jia *et al*. 2013), Waste alum sludge 10 g/L; (Babatunde and Zhao 2010)).

4. Conclusions

This study suggests the recycling of MVS as a value-added product for removing phosphate in aqueous solutions; it was thermally activated to enhance its phosphate adsorption capacity. The mineral composition of thermally activated MVS showed that $CaCO_3$ in MVS was decomposed into CaO at >700 °C because CO_2 was released. The C content of MVS decreased, and the Ca content increased. By comparing the phosphate adsorption capacity of each calcined adsorbent at each temperature of MVS, the optimum thermal treatment temperature of MVS to improve the phosphate adsorption capacity was determined to be 800 °C. MVS-800 suggested an adsorption mechanism through calcium phosphate precipitation. Subsequently, kinetic studies performed with MVS-800 showed that the PFO model was more suitable than the PSO model. In the equilibrium adsorption experiment, as a result of the analysis using the Langmuir and Freundlich models, Langmuir was able to provide a more appropriate explanation for the phosphate adsorption of MVS-800. This means that all surface areas were homogeneous for phosphate adsorption by MVS-800, and the adsorption consisted of a single layer. Compared with the phosphate adsorbents reported in the literature, the maximum adsorption capacity (194.22 mg/g) of MVS-800 appears to be high. Thermodynamic analysis of thermally activated MVS-800 showed that phosphate adsorption was an endothermic and involuntary reaction. Phosphate adsorption by MVS-800 was highest at low pH. The presence of anions in the phosphate adsorption decreased the phosphate adsorption of MVS-800 in the order of CO_3^{2-}, SO_4^{2-}, NO_3^-, and Cl^-. The optimal injection amount for phosphate adsorption on MVS-800 was determined to be 6.67 g/L. According to the experimental data thus far, MVS-800 is an eco-friendly adsorbent that recycles waste resources, and it is judged to be an adsorbent with high adsorption power to remove phosphate from aqueous solutions.

Acknowledgments

This work was studied with the support of the joint research project (No. PJ016998) of the Rural Development Administration (RDA).

References

Babatunde, A.O. and Zhao, Y.Q. (2010), "Equilibrium and kinetic analysis of phosphates adsorption from aqueous solution using waste alum sludge", *J. Hazard. Mater.*, **184**(1-3), 746-752. https://doi.org/10.1016/j.jhazmat.2010.08.102.

Barron, V., Herruzo, M. and Torrent, J. (1988), "Phosphate adsorption by aluminous hematites of different shapes", *Soil Sci. Soc. Am. J*, **52**(3), 647-651. https://doi.org/10.2136/sssaj1988.03615995005200030009x.

Bhagowati, B. and Ahamad, K.U. (2019), "A review on lake eutrophication dynamics and recent developments in lake modeling", *Ecohydrol. Hydrobiol.*, **19**(1), 155-166. https://doi.org/10.1016/j.ecohyd.2018.03.002.

Chen, J.P., Chua, M.L. and Zhang, B. (2002), "Effects of competitive ions, humic acid, and pH on removal of ammonium and phosphorous from the synthetic industrial effluent by ion exchange resins", *Waste Manage*, **22**(7), 711-719. https://doi.org/10.1016/S0956-053X(02)00051-X.

Cheng, G., Li, Q., Su, Z., Sheng, S. and Fu, J. (2018), "Preparation, optimization, and application of sustainable ceramsite substrate from coal fly ash/waterworks sludge/oyster shell for phosphorus immobilization in constructed wetlands", *J. Clean. Prod.*, **175**, 572-581. https://doi.org/10.1016/j.jclepro.2017.12.102.

Choi, M.Y., Lee, J.I., Lee, C.G. and Park, S.J. (2021), "Feasibility of using calcined Patinopecten yessoensis shells for fluoride removal and investigation of the fluoride removal mechanism", *Desalin Water Treat*, **233**, 292-302. https://doi.org/10.5004/dwt.2021.27551.

Christou, C., Philippou, K., Krasia-Christoforou, T. and Pashalidis, I. (2019), "Uranium adsorption by polyvinylpyrrolidone/ chitosan blended nanofibers", *Carbohydr. Polym.*, **219**, 298-305. https://doi.org/10.1016/j.carbpol.2019.05.041.

Clark, T., Stephenson, T. and Pearce, P.A. (1997), "Phosphates removal by chemical precipitation in a biological aerated

filter", *Water Res*., **31**(10), 2557-2563. https://doi.org/10.1016/S0043-1354(97)00091-2.

Currie, J.A., Harrison, N.R., Wang, L., Jones, M.I. and Brooks, M.S. (2007), "A preliminary study of processing seafood shells for eutrophication control", *Asia-Pac. J. Chem. Eng*., **2**(5), 460-467. https://doi.org/10.1002/apj.82.

Dos Reis, G.S., Cazacliu, B.G., Correa, C.R., Ovsyannikova, E., Kruse, A., Sampaio, C.H. and Dotto, G. L. (2020), "Adsorption and recovery of phosphate from aqueous solution by the construction and demolition wastes sludge and its potential use as phosphate-based fertilizer", *J. Environ. Chem. Eng*., **8**(1), 103605 https://doi.org/10.1016/j.jece.2019.103605.

Dos Reis, G.S., Thue, P.S., Cazacliu, B.G., Lima, E.C., Sampaio, C.H., Quattrone, M. and Dotto, G.L. (2020), "Effect of concrete carbonation on phosphate removal through adsorption process and its potential application as fertilizer", *J. Clean. Prod*., **256**, 120416. https://doi.org/10.1016/j.jclepro.2020.120416.

Du, X., Cheng, Y., Liu, Z., Yin, H., Wu, T., Huo, L. and Shu, C. (2021), "CO_2 and CH_4 adsorption on different rank coals: A thermodynamics study of surface potential, Gibbs free energy change and entropy loss", *Fuel*, **283**, 118886. https://doi.org/10.1016/j.fuel.2020.118886.

Dwivedi, C., Pathak, S.K., Kumar, M., Tripathi, S.C. and Bajaj, P.N. (2015), "Preparation and characterization of potassium nickel hexacyanoferrate-loaded hydrogel beads for the removal of cesium ions", *Environ. Sci. Water Res. Technol*., **1**(2), 153-160. https://doi.org/10.1039/C4EW00021H.

Fang, L., Wu, B. and Lo, I.M. (2017), "Fabrication of silica-free superparamagnetic ZrO_2@ Fe_3O_4 with enhanced phosphate recovery from sewage: Performance and adsorption mechanism", *Chem. Eng. J*., **319**, 258-267. https://doi.org/10.1016/j.cej.2017.03.012.

Gerke, J. (1993), "Phosphate adsorption by humic/Fe-oxide mixtures aged at pH 4 and 7 and by poorly ordered Fe-oxide", *Geoderma*, **59**(1-4), 279-288. https://doi.org/10.1016/0016-7061(93)90074-U.

Guaya, D., Valderrama, C., Farran, A., Armijos, C. and Cortina, J.L. (2015), "Simultaneous phosphate and ammonium removal from aqueous solution by a hydrated aluminum oxide modified natural zeolite", *Chem. Eng. J*., **271**, 204-213. https://doi.org/10.1016/j.cej.2015.03.003.

Hao, H., Wang, Y. and Shi, B. (2019), "NaLa $(CO_3)_2$ hybridized with Fe_3O_4 for efficient phosphate removal: synthesis and adsorption mechanistic study", *Water Res*., **155**, 1-11. https://doi.org/10.1016/j.watres.2019.01.049.

Hong, S.H., Lyonga, F.N., Kang, J.K., Seo, E.J., Lee, C.G., Jeong, S. and Park, S.J. (2020), "Synthesis of Fe-impregnated biochar from food waste for Selenium (VI) removal from aqueous solution through adsorption: Process optimization and assessment", *Chemosphere*, **252**, 126475. https://doi.org/10.1016/j.chemosphere.2020.126475.

Jia, C., Dai, Y., Chang, J.J., Wu, C., Wu, Z.B. and Liang, W. (2013), "Adsorption characteristics of used brick for phosphates removal from phosphate solution", *Desalin. Water Treat*., 51(28-30), 5886-5891. https://doi.org/10.1080/19443994.2013.770207.

Jiao, G.J., Ma, J., Li, Y., Jin, D., Guo, Y., Zhou, J. and Sun, R. (2021), "Enhanced adsorption activity for phosphate removal by functional lignin-derived carbon-based adsorbent: Optimization, performance and evaluation", *Sci. Total. Environ*, **761**, 143217. https://doi.org/10.1016/j.scitotenv.2020.143217.

Karaca, S., Gürses, A., Ejder, M. and Açıkyıldız, M. (2006), "Adsorptive removal of phosphate from aqueous solutions using raw and calcinated dolomite", *J. Hazard. Mater*., **128**(2-3), 273-279. https://doi.org/10.1016/j.jhazmat.2005.08.003.

Kim, J., Deng, Q. and Benjamin, M.M. (2008), "Simultaneous removal of phosphates and foulants in a hybrid coagulation/ membrane filtration system", *Water Res.*, **42**(8-9), 2017-2024. https://doi.org/10.1016/j.watres.2007.12.017.

Kumar, E., Bhatnagar, A., Hogland, W., Marques, M. and Sillanpää, M. (2014), "Interaction of inorganic anions with iron-mineral adsorbents in aqueous media—A review", *Adv. Colloid Interf. Sci*., **203**, 11-21. https://doi.org/10.1016/j.cis.2013.10.026.

Kumar, I.A. and Viswanathan, N. (2018), "A facile synthesis of magnetic particles sprayed gelatin embedded hydrotalcite composite for effective phosphate sorption", *J. Environ. Chem. Eng*., **6**(1), 208-217. https://doi.org/10.1016/j.jece.2017.11.042.

Lee, J.I., Kang, J.K., Oh, J.S., Yoo, S.C., Lee, C.G., Jho, E.H. and Park, S J. (2021), "New insight to the use of oyster shell for removing phosphorus from aqueous solutions and fertilizing rice growth", *J. Clean. Prod*., **328**, 129536. https://doi.org/10.1016/j.jclepro.2021.129536.

Lee, J.I., Kim, J.M., Yoo, S.C., Jho, E.H., Lee, C.G. and Park, S.J. (2022). "Restoring phosphates from water to soil: Using calcined eggshells for P adsorption and subsequent application of the adsorbent as a P fertilizer", *Chemosphere*, **287**, 132267. https://doi.org/10.1016/j.chemosphere.2021.132267.

Lee, J.I., Oh, J.S., Yoo, S.C., Jho, E.H., Lee, C.G. and Park, S.J. (2022), "Removal of phosphorus from water using calcium-rich organic waste and its potential as a fertilizer for rice growth", *J. Environ. Chem. Eng*., **10**(2), 107367. https://doi.org/10.1016/j.jece.2022.107367.

Lima, E.C., Hosseini-Bandegharaei, A., Moreno-Piraján, J.C. and Anastopoulos, I. (2019), "A critical review of the estimation of the thermodynamic parameters on adsorption equilibria. Wrong use of equilibrium constant in the Van't Hoof equation for calculation of thermodynamic parameters of adsorption", *J. Mol. Liq*., **273**, 425-434. https://doi.org/10.1016/j.molliq.2018.10.048.

Liu, H., Sun, X., Yin, C. and Hu, C. (2008), "Removal of phosphate by mesoporous ZrO_2", *J. Hazard. Mater*., **151**(2-3), 616-622. https://doi.org/10.1016/j.jhazmat.2007.06.033.

Liu, J., Wan, L., Zhang, L. and Zhou, Q. (2011), "Effect of pH, ionic strength, and temperature on the phosphate adsorption onto lanthanum-doped activated carbon fiber", *J. Colloid Interf. Sci*., **364**(2), 490-496. https://doi.org/10.1016/j.jcis.2011.08.067.

Liu, J., Zhou, Q., Chen, J., Zhang, L. and Chang, N. (2013), "Phosphate adsorption on hydroxyl–iron–lanthanum doped activated carbon fiber", *Chem. Eng. J*., **215**, 859-867. https://doi.org/10.1016/j.cej.2012.11.067.

Liu, X. and Zhang, L. (2015), "Removal of phosphate anions using the modified chitosan beads: Adsorption kinetic, isotherm and mechanism studies", *Powder Technol*., **277**, 112-119. https://doi.org/10.1016/j.powtec.2015.02.055.

Liu, X., Shen, F. and Qi, X. (2019), "Adsorption recovery of phosphate from aqueous solution by CaO-biochar composites prepared from eggshell and rice straw", *Sci. Total Environ*., **666**, 694-702. https://doi.org/10.1016/j.scitotenv.2019.02.227.

Lo Monaco, P.A., Matos, A.T., Eustáquio Júnior, V., Ribeiro, I.C. and Teixeira, D.L. (2012), "Utilization of ground clam shells in the adsorption of phosphates and for correction of soil acidity", *Engenharia Agrícola*, **32**(5), 866-874. https://doi.org/10.1590/S0100-69162012000500006.

Long, F., Gong, J.L., Zeng, G.M., Chen, L., Wang, X.Y., Deng, J.H. and Zhang, X.R. (2011). "Removal of phosphate from aqueous solution by magnetic Fe–Zr binary oxide", *Chem. Eng. J*., 171(2), 448-455. https://doi.org/10.1016/j.cej.2011.03.102.

Luo, W., Hai, F.I., Price, W.E., Guo, W., Ngo, H.H., Yamamoto, K. and Nghiem, L.D. (2016), "Phosphates and water recovery by a novel osmotic membrane bioreactor–reverse osmosis system", *Bioresour. Technol*., **200**, 297-304. https://doi.org/10.1016/j.biortech.2015.10.029.

McBride, M.B. (1997), "A critique of diffuse double layer models applied to colloid and surface chemistry", *Clays Clay Miner.*, **45**(4), 598-608. https://doi.org/10.1346/CCMN.1997.0450412.

Morse, G.K., Brett, S.W., Guy, J.A. and Lester, J.N. (1998), "Review: Phosphates removal and recovery technologies", *Sci. Total. Environ*, **212**(1), 69-81. https://doi.org/10.1016/S0048-9697(97)00332-X.

Nguyen, T.A.H., Ngo, H.H., Guo, W.S., Nguyen, T.T., Vu, N.D., Soda, S. and Cao, T.H. (2020), "White hard clam (Meretrix lyrata) shells as novel filter media to augment the phosphates removal from wastewater", *Sci. Total. Environ*, **741**, 140483. https://doi.org/10.1016/j.scitotenv.2020.140483.

Ni, G., Li, Q., Kong, L. and Yu, H. (2015), "Mitochondrial phylogeography of a surf clam Mactra veneriformis in the East China Sea: Genetic homogeneity across two biogeographic boundaries", *Biochem. Syst. Ecol.*, **61**, 493-500. https://doi.org/10.1016/j.bse.2015.07.026.

Pan, G., Lyu, T. and Mortimer, R. (2018), "Comment: Closing phosphorus cycle from natural waters: Re-capturing phosphorus through an integrated water-energy-food strategy", *J. Environ. Sci.*, **65**, 375-376.

Plazinski, W., Rudzinski, W. and Plazinska, A. (2009), "Theoretical models of sorption kinetics including a surface reaction mechanism: A review", *Adv. Colloid Interf. Sci.*, **152**(1-2), 2-13. https://doi.org/10.1016/j.cis.2009.07.009.

Ren, Z., Jia, B., Zhang, G., Fu, X., Wang, Z., Wang, P. and Lv, L. (2021), "Study on adsorption of ammonia nitrogen by iron-loaded activated carbon from low temperature wastewater", *Chemosphere*, **262**, 127895. https://doi.org/10.1016/j.chemosphere.2020.127895.

Sağlam, A., Yetişsin, F., Demiralay, M. and Terzi, R. (2016), "Chapter 2-Copper Stress and Responses in Plants A2-Ahma, Parvaiz. Plant Metal Interaction", 21-40.

Sağlam, A., Yetişsin, F., Demiralay, M. and Terzi, R. (2016), "Chapter 2-copper stress and responses in plants A2-Ahma, Parvaiz", *Plant Metal Interact.*, 21-40. https://doi.org/10.1016/B978-0-12-803158-2.00002-3.

Shafqat, M.N. and Pierzynski, G.M. (2014). "The Freundlich adsorption isotherm constants and prediction of phosphorus bioavailability as affected by different phosphorus sources in two Kansas soils", *Chemosphere*, **99**, 72-80. https://doi.org/10.1016/j.chemosphere.2013.10.009.

Shin, H., Tiwari, D. and Kim, D.J. (2020), "Phosphate adsorption/ desorption kinetics and P bioavailability of Mg- biochar from ground coffee waste", *J. Water Process Eng.*, **37**, 101484. https://doi.org/10.1016/j.jwpe.2020.101484.

Sommariva, C., Converti, A. and Del Borghi, M. (1997), "Increase in phosphate removal from wastewater by alternating aerobic and anaerobic conditions", *Desalination*, **108**(1-3), 255-260. https://doi.org/10.1016/S0011-9164(97)00033-7.

Tan, I.A. W., Ahmad, A.L. and Hameed, B.H. (2008). "Adsorption of basic dye on high-surface-area activated carbon prepared from coconut husk: Equilibrium, kinetic and thermodynamic studies", *J. Hazard. Mater.*, **154**(1-3), 337-346. https://doi.org/10.1016/j.jhazmat.2007.10.031.

Triantafyllidis, K.S., Peleka, E.N., Komvokis, V.G. and Mavros, P.P. (2010), "Iron-modified hydrotalcite-like materials as highly efficient phosphate sorbents", *J. colloid Interface Sci.*, **342**(2), 427-436. https://doi.org/10.1016/j.jcis.2009.10.063.

Unuabonah, E.I., Adebowale, K.O. and Olu-Owolabi, B.I. (2007), "Kinetic and thermodynamic studies of the adsorption of lead (II) ions onto phosphate-modified kaolinite clay", *J. Hazard. Mater.*, **144**(1-2), 386-395. https://doi.org/10.1016/j.jhazmat.2006.10.046.

Wang, B., Xin, M., Wei, Q. and Xie, L. (2018), "A historical overview of coastal eutrophication in the China Seas", *Mar. Pollut. Bull.*, **136**, 394-400. https://doi.org/10.1016/j.marpolbul.2018.09.044.

Wang, C., Boithias, L., Ning, Z., Han, Y., Sauvage, S., Sánchez-Pérez, J.M. and Hatano, R. (2017), "Comparison of Langmuir and Freundlich adsorption equations within the SWAT-K model for assessing potassium environmental losses at basin scale", *Agric. Water Manag.*, **180**, 205-211. https://doi.org/10.1016/j.agwat.2016.08.001.

Wang, S., Kong, L., Long, J., Su, M., Diao, Z., Chang, X. and Shih, K. (2018), "Adsorption of phosphates by calcium-flour biochar: Isotherm, kinetic and transformation studies", *Chemosphere*, **195**, 666-672. https://doi.org/10.1016/j.chemosphere.2017.12.101.

Xiong, W., Tong, J., Yang, Z., Zeng, G., Zhou, Y., Wang, D. and Cheng, M. (2017), "Adsorption of phosphate from aqueous solution using iron-zirconium modified activated carbon nanofiber: Performance and mechanism", *J. colloid Interface Sci.*, **493**, 17-23. https://doi.org/10.1016/j.jcis.2017.01.024.

Yang, F., Zhang, S., Sun, Y., Tsang, D.C., Cheng, K. and Ok, Y.S. (2019). "Assembling biochar with various layered double hydroxides for enhancement of phosphorus recovery", *J. Hazard. Mater.*, **365**, 665-673. https://doi.org/10.1016/j.jhazmat.2018.11.047.

Yang, Q., Wang, X., Luo, W., Sun, J., Xu, Q., Chen, F. and Zeng, G. (2018), "Effectiveness and mechanisms of phosphate adsorption on iron-modified biochars derived from waste activated sludge", *Bioresour. Technol.*, **247**, 537-544. https://doi.org/10.1016/j.biortech.2017.09.136.

Ye, Z.L., Chen, S.H., Wang, S.M., Lin, L.F., Yan, Y.J., Zhang, Z.J. and Chen, J.S. (2010), "Phosphates recovery from synthetic swine wastewater by chemical precipitation using response surface methodology", *J. Hazard. Mater.*, **176**(1-3), 1083-1088. https://doi.org/10.1016/j.jhazmat.2009.10.129.

Yeoman, S., Stephenson, T., Lester, J.N. and Perry, R. (1988), "The removal of phosphates during wastewater treatment: A review", *Environ. Pollut.*, **49**(3), 183-233. https://doi.org/10.1016/0269-7491(88)90209-6.

Yin, H. and Kong, M. (2014), "Simultaneous removal of ammonium and phosphate from eutrophic waters using natural calcium-rich attapulgite-based versatile adsorbent", *Desalination*, **351**, 128-137. https://doi.org/10.1016/j.desal.2014.07.029.

Yu, J.H., Song, J.H., Choi, M.C. and Park, S.W. (2009), "Effects of water temperature change on immune function in surf clams, Mactra veneriformis (Bivalvia: Mactridae)", *J. Invertebr. Pathol.*, **102**(1), 30-35. https://doi.org/10.1016/j.jip.2009.06.002.

Zhang, M., Song, G., Gelardi, D.L., Huang, L., Khan, E., Mašek, O. and Ok, Y.S. (2020), "Evaluating biochar and its modifications for the removal of ammonium, nitrate, and phosphate in water", *Water Res.*, **186**, 116303. https://doi.org/10.1016/j.watres.2020.116303.

SP